Nov 6th, 12:00 AM - 12:00 AM

Strain and Stress Distributions in Composite Deck Slabs: A Numerical Study

Vitaliy V. Degtyarev

Twenty-Second International Specialty Conference on Cold-Formed Steel Structures
St. Louis, Missouri, USA, November 5 & 6, 2014

Strain and Stress Distributions in Composite Deck Slabs: A Numerical Study

Vitaliy V. Degtyarev[1]

Abstract

This paper describes results of a study on strain and stress distributions in compact and slender composite deck slabs using nonlinear three-dimensional finite element models. The slabs were modeled as flexural members made of steel deck units and structural concrete fillings interconnected at the interface with nonlinear springs representing bond between two materials. The models are capable of accounting for partial interaction between the deck and the concrete, discrete concrete cracking in the slab tension zone, and nonlinear behavior of the materials and the interface. They were validated against published test data and have proved to be effective in predicting load-deflection responses of composite deck slabs. The study showed that the strain and stress distributions are greatly affected by concrete cracking and slip between the deck and the concrete. The study provides information that may be useful in understanding composite slab behavior and in developing analytical models for predicting slab strength and stiffness.

Introduction

Concrete slabs over steel composite decks are widely used in steel-framed buildings. The slabs are designed as steel-concrete composite slabs with the deck acting as positive external reinforcement. Strength and behavior of composite slabs have been investigated by many researchers both experimentally and numerically. References to the papers describing the studies can be found in Yu and LaBoube (2010).

The vast majority of studies conducted to date have focused on slab strength and load-deflection response. Relatively little research has been reported on strain and stress distributions in steel-deck-reinforced composite slabs. Only one paper was found that contained detailed experimental data on strain and stress distributions in composite slabs at different behavior stages (Chen et al. 2011).

[1] Senior Design Engineer, Metal Dek Group, a unit of CSi, Columbia, SC, USA

While the importance of the experimental results cannot be overemphasized, they may not give a full picture of the stress-strain state of a composite slab due to technical difficulties in obtaining such data from tests. Finite element analysis (FEA) may supplement the laboratory testing and significantly reduce the number of experiments.

FEA has been used by several researchers to investigate the behavior of composite slabs (Abdullah and Easterling 2009, Chen and Shi 2011, Daniels and Crisinel 1993, Tsalkatidis and Avdelas 2010, Veljkovic 1998, and Widjaja 1997). The published numerical studies, however, have also focused on slab strength and load-deflection behavior and provided limited data on strain and stress distributions in the slabs.

Available slab design methods are either semi-empirical, which require a large number of tests, or analytical developed using simplified assumptions, which in some cases may not be capable of capturing the important characteristics affecting slab strength and behavior. The knowledge of strain and stress distributions in deck-reinforced composite slabs is essential for understanding slab behavior and developing accurate and reliable analytical models and design methods.

The objective of this paper is to present results of a study on strain and stress distributions in compact and slender composite deck slabs using nonlinear three-dimensional FE models, which are capable of accounting for partial interaction between the deck and the concrete, discrete concrete cracking in the slab tension zone, and nonlinear behavior of the materials and the interface.

Numerical study program

The numerical study described in this paper was performed on nonlinear three-dimensional FE models of two composite slabs tested by Abdullah (2004). The modeled slabs consisted of a 0.0598 in. (1.5 mm) thick 2 in. (51 mm) deep trapezoidal composite deck with 2 in. (51 mm) and 4½ in. (114 mm) normal weight concrete topping. The 6½ in. (165 mm) and 4 in. (102 mm) deep slabs are referred to as the compact and slender slabs, respectively. Table 1 shows main properties of the modeled slabs. All other test specimen and test procedure details can be found in Abdullah (2004).

Table 1. Main properties of modeled slabs

Slab Type	Test ID	h, in. (mm)	L, in. (mm)	L_V, in. (mm)	f_y, ksi (MPa)	f'_c, ksi (MPa)
Compact	2VL16-7-6.5	6.5 (165)	84 (2134)	28 (711)	47 (324)	4.5 (31)
Slender	2VL16-12-4	4.0 (102)	144 (3658)	46 (1168)	47 (324)	4.3 (30)

Notes: h is total slab depth; L is center-to-center span length; L_V is shear span length; f_y is yield strength of deck steel; f'_c is concrete compressive strength.

Finite element model description

For evaluating the realistic behavior of composite slabs under vertical loads, the following critical parameters were accounted for in the models: partial interaction between the deck and the concrete, concrete cracking in the slab tension zone, and nonlinear stress-strain relationships of the steel, the concrete, and the interface. Due to the symmetric conditions, only one-half of a one foot wide slab strip was modeled. Fig. 1 shows typical FE meshes for the compact and slender slabs.

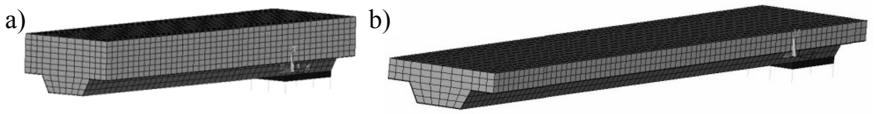

Fig. 1. Finite element model of a) compact slab and b) slender slab

The concrete was modeled with eight-node 3D reinforced concrete solid elements SOLID65, which are capable of plastic deformations, cracking in tension, and crushing in compression. The element cracking is treated as "a smeared band" of cracks in ANSYS. The multilinear isotropic hardening plasticity (MISO) of concrete in compression was combined with the William-Warnke failure criterion (William and Warnke, 1975) in tension to model the nonlinear material behavior of concrete. The uniaxial stress-strain relationships for concrete in compression were obtained using the Desayi and Krishnan model (Desayi and Krishnan 1964) not accounting for the descending branch of the curve: $f_c = (E_c\varepsilon_c)/(1 + (\varepsilon_c/\varepsilon_0)^2)$, where f_c is stress at any strain ε_c; $\varepsilon_0 = 2f'_c/E_c$ is strain at the concrete compressive strength f'_c; $E_c = w_c^{1.5}\sqrt{f'_c}$ (f'_c is in ksi) is concrete initial tangent modulus; w_c is unit weight of concrete. Values of f'_c and w_c for each tested slab are published in Abdullah (2004). To improve convergence, the crushing capability of concrete was turned off as suggested by Kachlakev et al. (2001) and Queiroz et al. (2007). Concrete cracked in tension whenever a principal stress component exceeded concrete ultimate uniaxial tensile strength f_{ct} calculated as $f_{ct} = 7.5\sqrt{f'_c}$ (f'_c is in psi) (ACI 318 2008). The shear transfer coefficient β_t represents a shear strength reduction factor in a cracked section and depends on the crack face roughness. It ranges from 0 for a smooth crack, which does not transfer shear, to 1 for a rough crack, which transfers shear without loss. Shear transfer coefficients of 0.3 and 1.0 were used in this study for open and closed cracks, respectively. The concrete was assumed to have a Poisson's ratio of 0.2.

The steel deck and the steel support plate were modeled with eight-node 3D structural solid elements SOLID45. No embossments were modeled on the deck

surface. The multilinear isotropic hardening material model (MISO) was used for the deck, which was assumed to be elastic until the yield stress was reached and elasto-plastic in the stress range between the yield stress and ultimate strength. An elastic modulus of 29500 ksi ($2.03 \cdot 10^5$ MPa) and a Poisson's ratio of 0.3 were used for the deck. The engineering yield stress, ultimate strength, and ultimate strain were taken from Abdullah (2004). The engineering yield strain was calculated as a ratio of the engineering yield stress to the elastic modulus. The engineering stresses and strains were converted into true stresses and strains and entered into the models.

Tested slabs were supported by W21×68 beams, only the top flange of which was modeled as a steel supporting plate. The plate was assumed to be elastic-perfectly plastic with a Poisson's ratio of 0.3, an elastic modulus of 29000 ksi ($2 \cdot 10^5$ MPa), and a yield strength of 50 ksi (345 MPa).

Flexible-flexible contact pairs consisting of TARGE170 3-D target segments and CONTA173 3-D 4-node surface-to-surface contacts were created between the following surfaces: the deck top flange and the concrete, the deck bottom flange and the concrete, each deck web and the concrete, and the deck bottom flange and the supporting plate. All the contacts were frictionless except for the deck bottom flange-to-concrete contact over the supporting plate and the deck bottom flange-to-supporting plate contact, which were friction contacts with an interface coefficient of friction of 0.6. The Coulomb friction model was used. All the contacts were modeled as "no separation" contacts except for the deck bottom flange-to-supporting plate contact, which was modeled as a standard unilateral contact. In "no separation" contacts, the target and contact surfaces are tied together during the analysis, while sliding is permitted. Standard unilateral contacts allow for separation of the surfaces.

The separation between the deck bottom flange and the supporting plate was allowed in the models because testing showed that the deck attachment to the supporting beam failed at some point during the tests, after which the slab end rotated and was bearing only on the beam flange edge (Abdullah 2004). The deck attachment to the beam was modeled with eight COMBIN39 nonlinear spring elements installed between the deck bottom flange and the supporting plate. The force-deflection curve of the COMBIN39 elements was determined for each slab during model calibration. This approach allowed the author to capture the slab end rotation and bearing on the beam flange edge observed in the tests (Fig. 2).

Only webs of the tested composite deck profiles were embossed. Therefore, the mechanical interlock between the deck and concrete was modeled with

COMBIN39 elements at two interfaces between the deck webs and concrete. Nonlinear force-deflection curves of the COMBIN39 elements were specified and calibrated against test data.

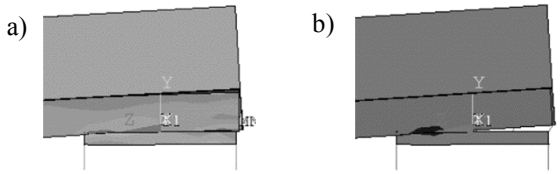

Fig. 2. Slab bearing at support: a) before deck-to-support attachment failure; b) after deck-to-support attachment failure

A single line of nodes at the center of the supporting plate bottom face was restricted from translations in all three directions. Stiffeners were welded to the webs and flanges of the supporting beams in the tests. Therefore, it was assumed that the beam flanges were restrained against rotation. To model the restraint, one end of COMBIN14 spring-damper elements with a relatively high spring constant of 10^{10} lbs/in ($1.75 \cdot 10^{10}$ kN/m) was attached to the plate edges while another end of the elements was restrained from translations in the directions parallel to the slab depth and width. The plate end translation in the direction parallel to the slab width was restrained to prevent plate rotation. To model the symmetry, the deck and concrete nodes at the center of the slab were restrained from translation in the direction parallel to the slab span. The deck and concrete nodes at the center of the slab were also restrained from translation in the direction parallel to the slab width.

The models were loaded by an imposed displacement applied in small increments to a node on the slab top face at the distance of L_v from the support center. Vertical displacements of the slab top face nodes at the distance of L_v from the support center were coupled, which resulted in the imposed displacement applied to all nodes on the slab top face at the distance of L_v from the support center. ANSYS uses the Newton-Raphson method to solve nonlinear equations. The L2 norm (square root sum of the squares) of force with a tolerance of 0.05 was used in this study.

Finite element model calibration and validation

Multiple analyses were performed for each model. Different force-deflection curves were tried for the COMBIN39 elements at the deck-concrete interface and between the deck and the supporting plate until reasonable agreements between the FEA and experimental load-deflection curves were achieved. The force-deflection curves determined from the calibration and corresponding shear bond stress-slip relationships are shown in Fig. 3. The shear bond stress values

were calculated as a COMBIN39 element force times the number of the elements at one deck web divided by the surface area of one deck web.

Fig. 4 shows comparisons between the load-deflection curves of the tested slabs and the FE models. The load is presented as equivalent uniform load as in Abdullah (2004). The equivalent uniform load was determined by equating the moments in the modeled slab to the moments in a uniformly loaded simply supported slab. As can be seen from Fig. 4, the FE models were able to predict the experimental slab behavior and strength reasonably well.

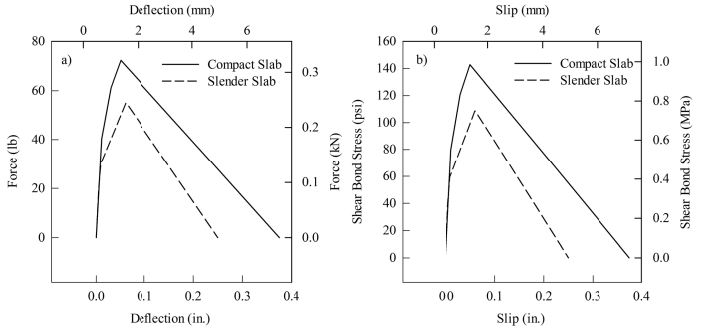

Fig. 3. a) Force-deflection curves for COMBIN39 elements at deck-concrete interface, b) shear bond stress-slip relationships

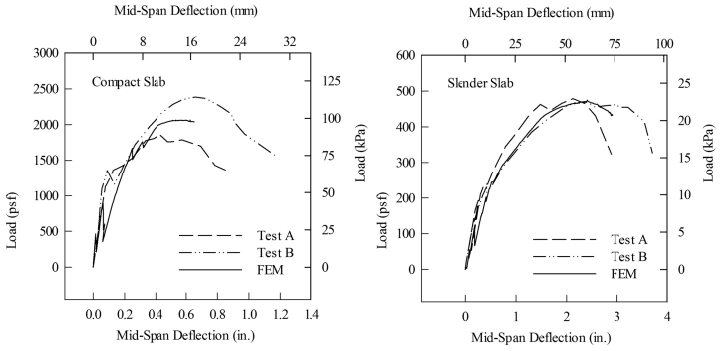

Fig. 4. Comparisons of load deflection curves of tested slabs and FE models

Numerical study results and discussion

Fig. 5 shows stress variations in the deck top and bottom flanges, as well as at the concrete top and bottom faces, along the half span. The deck and concrete stresses were normalized by deck yield strength and concrete compressive

strength, respectively. The deck stresses were averaged across the flange width and the deck thickness. The concrete top and bottom face stresses were averaged across the slab width and the concrete rib width at the bottom, respectively. The longitudinal slab coordinate with the origin at the center of the slab support was normalized by the span length. Each graph shows four lines representing stresses at four behavior stages: before concrete cracking, after concrete cracking, service stage, and ultimate stage. The ultimate stage corresponded to the maximum load supported by the slab models, whereas the service stage was assumed to correspond to 0.6 of the maximum load. Due to the slab rotational restraint at the support, the slab model portion near the support was in negative bending (see Fig. 5).

Concrete and deck strain distributions through the slab and deck depths in the cracked sections at the load application line (that is, in the major crack section) and in the sections between cracks are shown in Fig. 6. The strains were averaged across the slab width. Fig. 7 shows variations of slip between the deck and the concrete and shear bond forces at the deck-concrete interface, F_{bond}, along the half span. The slip and the shear bond forces were averaged across the slab width and through the deck height. The shear bond forces were normalized by the maximum shear bond forces, $F_{bond,max}$, for each slab. The strain and stress distributions at each behavior stage are analyzed further in the paper. The analysis relates to the constant moment region unless noted otherwise.

Strain and stress distributions in slabs before concrete cracking

Before concrete cracking, the stresses in the deck and in the concrete repeated the bending moment diagram. Slip between the deck and the concrete and shear bond forces were relatively small and zero at the slab mid-span. They increased towards the support and then decreased again near the support due to the slab rotational restraint used in the tests and in the models. Because of the small slip, the composite sections had one neutral axis; and the strain distributions conformed to the hypothesis of plane sections.

Strain and stress distributions in slabs after concrete cracking

The first flexural cracks occurred at the mid-span of both models. The first crack formation was accompanied by the transfer of tensile load from the concrete to the deck and the initiation of slip between the deck and the concrete in the cracked section. The bond forces increased significantly near the cracks. Due to the concrete cracking and the slip, one neutral axis developed in the concrete section and another in the deck section, which invalidated the plane section hypothesis in the slab cracked sections. The depth of the concrete compression zone significantly reduced after concrete cracking.

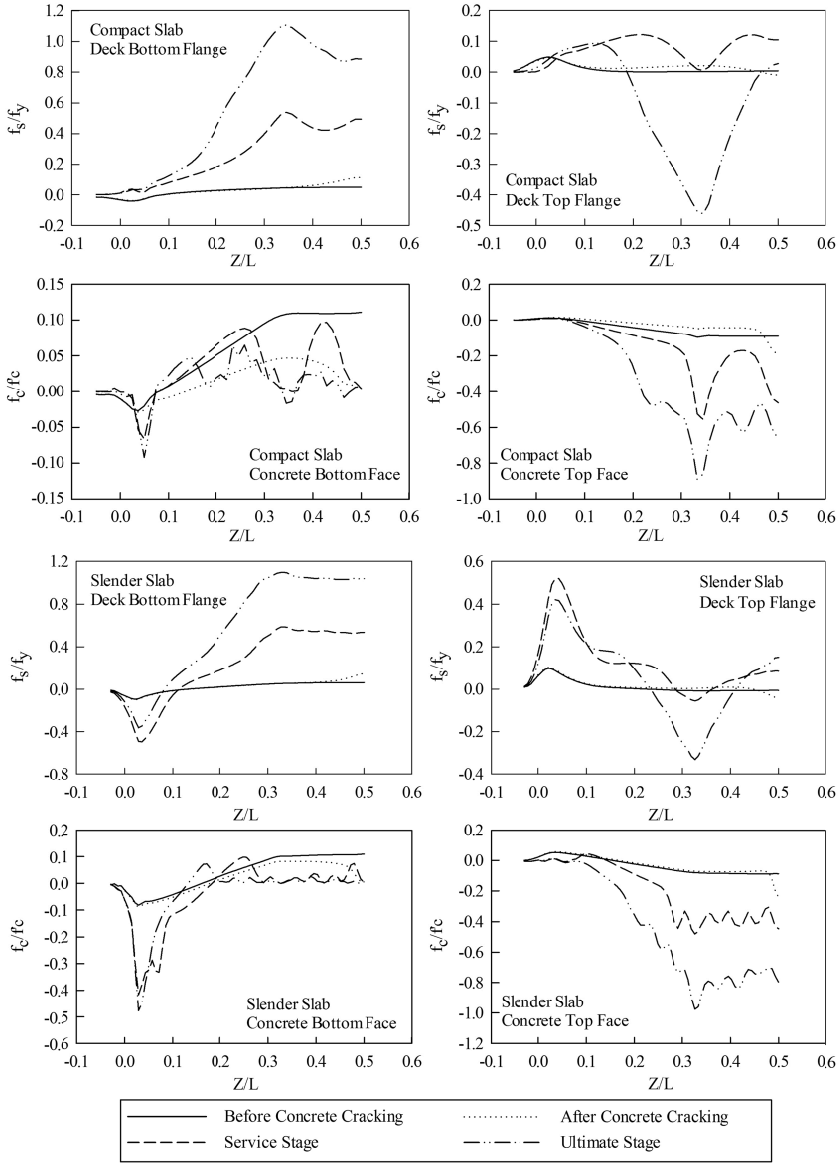

Fig. 5. Stress distributions in deck and concrete along half span

Notes: f_s is stress in steel deck; Z is the coordinate parallel to slab span

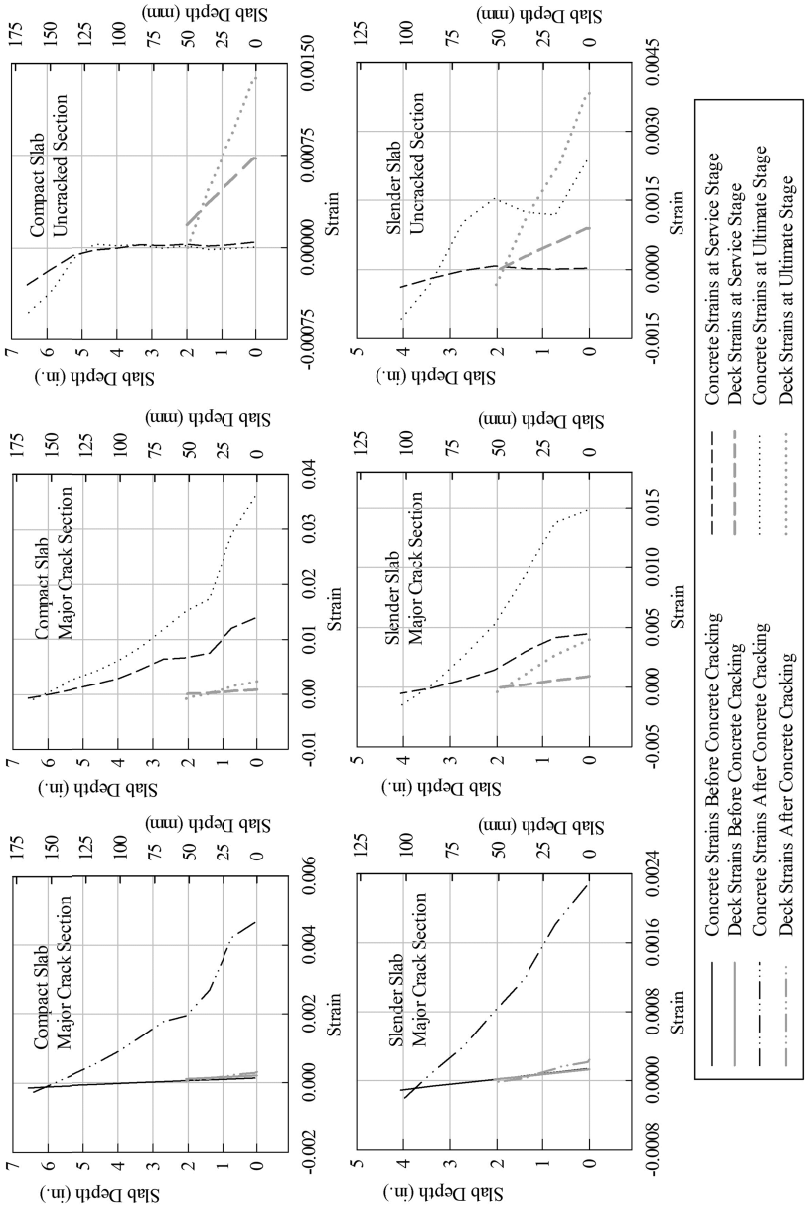

Fig. 6. Strain profiles in cracked and uncracked sections

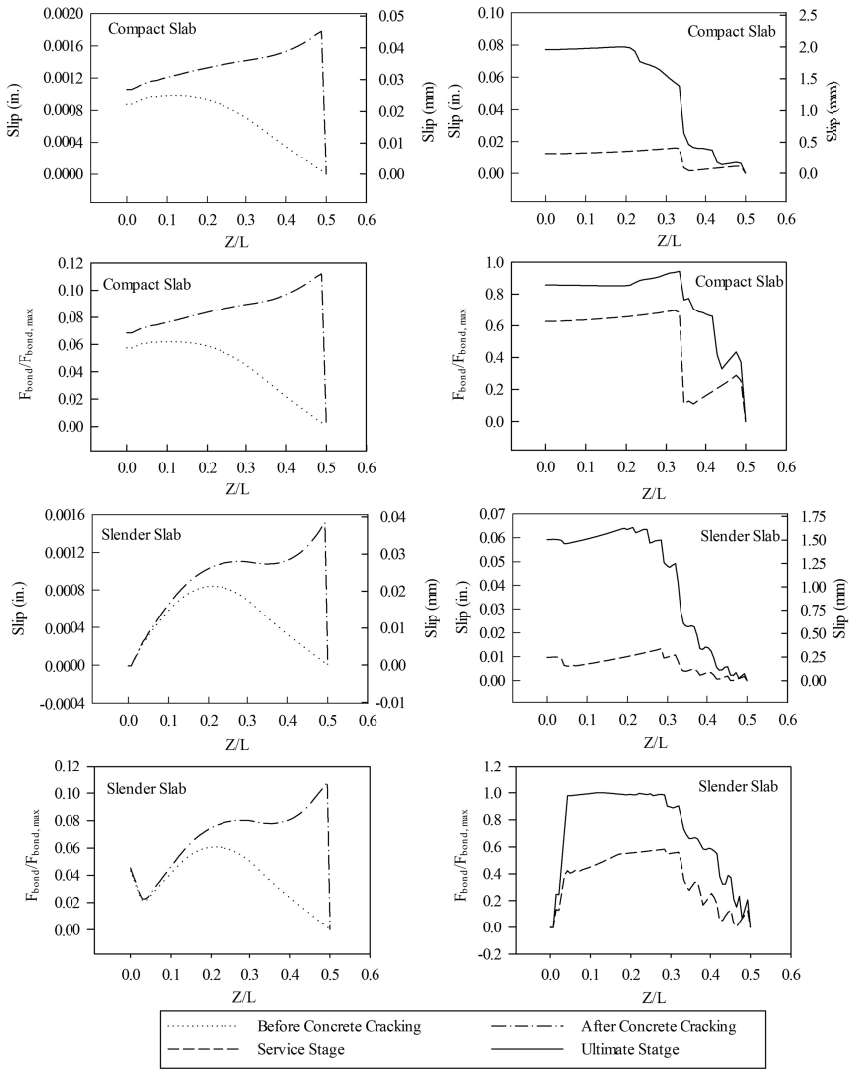

Fig. 7. Distribution of slip between deck and concrete and shear bond forces along half span

The following changes occurred in the deck and concrete stresses in the first crack section as a result of concrete cracking: the concrete bottom face stress reduced down to zero, the deck bottom flange and concrete top face stresses significantly increased, and the deck top flange stress changed from tension to compression. Bond between the deck and the concrete gradually transferred the tensile load back to the concrete on either side of the crack, which reduced the deck and concrete top face stresses at a distance from the crack.

Strain and stress distributions in slabs in service stage

As the load increased, more cracks developed in the models. Locations of the cracked sections along the half span correspond to the stress peaks in the concrete top face, which can be clearly seen in Fig. 5. This shows that the "smear band" crack approach used in the ANSYS SOLID65 element was capable of modeling discrete cracks in concrete and the effects of the discrete cracks on strain and stress distributions in composite deck slabs.

In the half of the constant moment region, the compact and slender slab models had two and five flexural cracks, respectively. The slender slab model also had one crack within the shear span. The average crack spacing for the compact and slender slab models in the constant moment region was 14 in. (356 mm) and 6.5 in. (165 mm), respectively. Slip between the deck and the concrete and shear bond forces increased abruptly in the cracked sections. Slip increments in the cracked sections, which correspond to crack widths, were smaller for the slender slab model. This implies that crack width in composite slabs increased with an increase in crack spacing. Slip and shear bond forces within the shear span were larger than those within the constant moment region for the compact and slender slab models.

The slab models had two neutral axes in the major crack sections. In the uncracked section of the slender slab model, only one neutral axis was observed and the plane sections hypothesis was valid, because of the relatively small slip between the deck and the concrete, which was approximately 0.003 in. (0.08 mm). The slip in the uncracked section of the compact slab model was approximately two times larger. As a result, the plane section hypothesis was invalid for the uncracked section of the compact slab model even though the slab had only one neutral axis. The concrete compression zone was deeper in the uncracked sections. These observations confirm the well-known facts that the degree of composite action is a function of slip between two materials and that the plane section hypothesis becomes invalid when the slip becomes large.

Variations of the deck bottom flange and concrete top face stresses in the compact slab model show two distinct peaks in the cracked sections. The deck bottom flange and concrete top face stresses varied from $0.54f_y$ and $0.56f'_c$, respectively, in the major crack section to $0.42f_y$ and $0.17f'_c$, respectively, in the sections between cracks. Due to closer crack spacing, the deck bottom flange stress and concrete top face stress variations were smaller in the slender slab model when compared with the compact slab model. In the slender slab model, the deck bottom flange and concrete top face stresses varied from $0.59f_y$ and $0.46f'_c$, respectively, in major crack section to $0.53f_y$ and $0.32f'_c$, respectively, in the sections between cracks.

The deck top flange stresses in both the compact and slender slab models reduced near the major crack. They were equal to zero in the compact slab model and changed from tension to compression in the slender slab model, whereas deck top flange away from the major crack section remained in tension. The deck top flange stresses varied from 0 to $0.12f_y$ in tension for the compact slab model and from $0.06f_y$ in compression to $0.09f_y$ in tension for the slender slab model. The concrete bottom face stresses in both models varied from zero in the cracked sections to the values approaching concrete tensile strength in the sections between cracks.

Strain and stress distributions in slabs in ultimate stage

In the half of the constant moment region, one more crack developed in the compact slab model and none in the slender slab model. One and two additional cracks appeared in each shear span of the compact and slender slab models, respectively. The average crack spacing in the constant moment region of the compact slab model became 7 in. (178 mm), while the average crack spacing in the constant moment region of the slender slab model did not change.

Slip between the deck and the concrete within the shear span increased approximately five times when compared to the service stage. Due to the significant slip increase, two neutral axes formed in both cracked and uncracked sections of the compact and slender slab models. Strain distributions did not conform to the plane section hypothesis. Shear bond forces within the shear span also increased and reached their ultimate values.

In the ultimate stage, the deck bottom flange stresses in the major crack sections of both the compact and slender slab models consisted approximately $1.10f_y$. In the sections between cracks, they reduced down to $0.87f_y$ and $1.03f_y$ in the compact and slender slab models, respectively. Thus, the deck bottom flange of the slender slab model yielded over the entire length of the constant moment

region, whereas the deck bottom flange stresses of the compact slab model reached yield strength only in the sections near the major crack. The deck top flange stress varied from $0.46f_y$ in compression to $0.03f_y$ in tension and from $0.32f_y$ in compression to $0.15f_y$ in tension for the compact and slender slab models, respectively. This demonstrates that deck stresses vary significantly along the constant moment region due to concrete cracking, slip, and nonlinear shear bond forces at the deck-concrete interface.

The concrete top face stresses varied along the constant moment region with the maximum values in the major crack section. They were $0.89f'_c$ and $0.98f'_c$ in the compact and slender slab models, respectively. The minimum values of the concrete compressive stresses within the constant moment region were $0.46f'_c$ and $0.71f'_c$ in the compact and slender slab models, respectively. The concrete bottom face stresses in both the compact and slender slab models were close to zero.

Conclusions

Nonlinear three-dimensional FE models of compact and slender composite deck slabs were developed in this study using the commercial software ANSYS. The models account for partial interaction between the deck and the concrete, concrete cracking in the slab tension zone, and nonlinear stress-strain relationships of the steel, the concrete, and the interface. They were validated against published test data and have proved to be effective in predicting load-deflection responses of compact and slender composite deck slabs. The "smear band" crack approach used in the ANSYS SOLID65 element was capable of modeling discrete cracks in concrete and the effects of the discrete cracks on strain and stress distributions in the slabs.

The FE study showed that strain and stress distributions in the composite deck slabs were greatly affected by concrete cracking and slip between the deck and the concrete. Deck and concrete strain distributions through the slab depth in cracked sections differed from those in uncracked sections. Due to slip, the composite sections had two neutral axes in most cases. The plane section hypothesis was invalid for cracked sections. It was valid only for uncracked sections when slip between the deck and the concrete was relatively small.

The deck bottom flange and concrete top face stresses had maximum values in the major crack sections. They also had peaks in other cracked sections, but the stress values were smaller than those in the major crack section. The minimum values of the deck bottom flange and the concrete top face stresses were observed in the sections between cracks. In the ultimate stage, the deck bottom

flange stresses of the slender slab model exceeded yield strength along the entire length of the constant moment region. In the compact slab models, they exceeded yield strength near the major crack section only. The concrete top face stresses were close to concrete compressive strength but did not reach it. As a result of concrete cracking and slip between the deck and the concrete, the deck top flange stresses changed from tension to compression in the major crack sections when the load approached the ultimate value. The deck top flange stresses varied from tension to compression along the slab constant moment region. The concrete bottom face stresses were equal to zero in cracked sections and approached concrete tensile strength in sections between cracks.

Shear bond forces were present in the constant moment region due to concrete cracking. Shear bond forces and slip were noticeably higher within the shear span when compared with the constant moment region. Slip between the deck and the concrete and shear bond forces increased abruptly in the cracked sections.

Acknowledgements

The author expresses his gratitude to South Ural State University and personally to Dr. Natalya Degtyareva for allowing the use of ANSYS available at the University.

References

Abdullah, R. (2004). "Experimental Evaluation and Analytical Modeling of Shear Bond in Composite Slabs," Ph.D. Thesis, Virginia Polytechnic Institute and State University, Blacksburg, VA.

Abdullah, R., and Easterling, W.S. (2009). "New evaluation and modeling procedure for horizontal shear bond in composite slabs." *Journal of Constructional Steel Research*, 65(4), 891-899.

ACI 318. (2008). *Building Code Requirements for Structural Concrete (ACI 318-08) and Commentary*, American Concrete Institute, Farmington Hills, MI.

ANSYS. (2007). Finite Element Computer Code. Version 11. ANSYS, Inc., Canonsburg, PA.

Chen, S., and Shi, X. (2011). "Shear bond mechanism of composite slabs—A universal FE approach." *Journal of Constructional Steel Research*, 67(10), 1475-1484.

Chen, S., Shi, X., and Qiu, Z. (2011). "Shear bond failure in composite slabs—a detailed experimental study." *Steel and Composite Structures*, 11(3), 233-250.

Daniels, B.J., and Crisinel, M. (1993). "Composite slab behavior and strength analysis. Part I: Calculation procedure." *Journal of Structural Engineering*, 119(1), 16-35.

Desayi, P., and Krishnan, S. (1964). "Equation for the stress-strain curve of concrete." *Journal of the American Concrete Institute*, 61(3), 345-350.

Kachlakev, D.I., Miller, T., Yim, S., Chansawat, K., and Potisuk, T. (2001). "Finite Element Modeling of Reinforced Concrete Structures Strengthened With FRP Laminates." *Final Report SPR 316,* United States Department of Transportation Federal Highway Administration and the Oregon Department of Transportation, Salem, OR.

Queiroz, F.D., Vellasco, P.C.G.S., and Nethercot, D.A. (2007). "Finite element modelling of composite beams with full and partial shear connection." *Journal of Constructional Steel Research*, 63(4), 505-521.

Tsalkatidis, T., and Avdelas, A. (2010). "The unilateral contact problem in composite slabs: Experimental study and numerical treatment." *Journal of Constructional Steel Research*, 66(3), 480-486.

Veljkovic, M. (1998). "Influence of load arrangement on composite slab behaviour and recommendations for design." *Journal of Constructional Steel Research*, 45(2), 149-178.

Willam, K. J., and Warnke, E. D. (1975). "Constitutive model for the triaxial behavior of concrete." *Proc., International Association for Bridge and Structural Engineering,* 19, 1-30.

Yu, W. W., and LaBoube, R. A. (2010). *Cold-Formed Steel Design,* John Wiley & Sons, New York, NY.